Article

Neuron

Relationships between Pupil Diameter and Neuronal Activity in the Locus Coeruleus, Colliculi, and Cingulate Cortex

Highlights

- Neural activity in monkey locus coeruleus (LC) reflects changes in pupil size
- These effects are found for evoked and spontaneous activity, LFPs, and spikes
- Some similar effects are found in LC-linked areas of colliculi and cingulate cortex
- Thus, LC-mediated arousal may coordinate neural activity in some parts of the brain

Authors

Siddhartha Joshi, Yin Li, Rishi M. Kalwani, Joshua I. Gold

Correspondence

sidjoshi@mail.med.upenn.edu

In Brief

Joshi et al. found that changes in pupil diameter can reflect neural activity in the locus coeruleus (LC) and, less reliably, several other interconnected structures. The results suggest that LC-mediated arousal may coordinate activity throughout some parts of the brain.

Joshi et al., 2016, Neuron *89*, 221–234
January 6, 2016
http://dx.doi.org/10.1016/j.neuron.2015.11.028

CellPress

Neuron
Article

Relationships between Pupil Diameter and Neuronal Activity in the Locus Coeruleus, Colliculi, and Cingulate Cortex

Siddhartha Joshi,[1,*] Yin Li,[1] Rishi M. Kalwani,[2] and Joshua I. Gold[1]
[1]Department of Neuroscience, University of Pennsylvania, Philadelphia, PA 19104, USA
[2]Temple University School of Medicine, Philadelphia, PA 19140, USA
*Correspondence: sidjoshi@mail.med.upenn.edu
http://dx.doi.org/10.1016/j.neuron.2015.11.028

SUMMARY

Changes in pupil diameter that reflect effort and other cognitive factors are often interpreted in terms of the activity of norepinephrine-containing neurons in the brainstem nucleus locus coeruleus (LC), but there is little direct evidence for such a relationship. Here, we show that LC activation reliably anticipates changes in pupil diameter that either fluctuate naturally or are driven by external events during near fixation, as in many psychophysical tasks. This relationship occurs on as fine a temporal and spatial scale as single spikes from single units. However, this relationship is not specific to the LC. Similar relationships, albeit with delayed timing and different reliabilities across sites, are evident in the inferior and superior colliculus and anterior and posterior cingulate cortex. Because these regions are interconnected with the LC, the results suggest that non-luminance-mediated changes in pupil diameter might reflect LC-mediated coordination of neuronal activity throughout some parts of the brain.

INTRODUCTION

Non-luminance-mediated changes in pupil diameter have long been used as markers of arousal and cognitive effort and, more recently, have been interpreted in terms of the explore-exploit trade-off, surprise, salience, decision biases, and other factors that can influence ongoing information processing (Jepma and Nieuwenhuis, 2011; Gilzenrat et al., 2010; Krugman, 1964; Granholm and Steinhauer, 2004; Schmidt and Fortin, 1982; Kahneman and Beatty, 1966; Richer and Beatty, 1987; Einhäuser et al., 2008; Alnæs et al., 2014; de Gee et al., 2014; Wang et al., 2014; Lavín et al., 2014; Eldar et al., 2013; Nassar et al., 2012; Takeuchi et al., 2011; Preuschoff et al., 2011; Einhäuser et al., 2010; McGinley et al., 2015). In many cases, these effects have been interpreted in terms of activation of norepinephrine (NE)-containing neurons in the brainstem nucleus locus coeruleus (LC). The proposed functional association between LC activation and pupil diameter is based largely on indirect evidence, including anatomical and pharmacological studies, fMRI and electroencephalogram (EEG) studies that measured both brain activity and pupil diameter, and common factors that drive LC and pupil changes (Phillips et al., 2000; Hou et al., 2005; Beatty, 1982a, 1982b; Richer and Beatty, 1987; Einhäuser et al., 2008; Gilzenrat et al., 2010; Morad et al., 2000; Aston-Jones and Cohen, 2005; Murphy et al., 2011, 2014). More direct evidence includes one commonly cited single-unit example (Aston-Jones and Cohen, 2005) and a recent report relating event-driven changes in LC spiking activity and pupil diameter in monkeys (Varazzani et al., 2015). Pupil diameter also can covary with neuronal activity in cortex, which is thought to reflect, at least in part, modulation by the LC-NE system (Vinck et al., 2015; Reimer et al., 2014; Ebitz and Platt, 2015; Eldar et al., 2013; McGinley et al., 2015). The goal of our study was to provide, for the first time, a direct and systematic examination of the timescale, magnitude, and prevalence of relationships between both spontaneous and event-driven changes in pupil diameter and neural activity in the LC and elsewhere in the brain.

We simultaneously measured pupil diameter and neural activity in several brain regions (recorded separately; Figure 1) of alert, fixating monkeys, either during passive viewing or in response to arousing sounds. We targeted the LC and adjacent NE-containing subcoeruleus, which, together, we refer to as LC+ (Kalwani et al., 2014), plus several other brain regions interconnected with the LC-NE system. The inferior colliculus (IC) receives dense projections from LC and, as part of the ascending auditory pathway, is sensitive to our sound manipulation (Klepper and Herbert, 1991; Hormigo et al., 2012; Foote et al., 1983; Levitt and Moore, 1978). The intermediate layer of superior colliculus (SC_i) also receives LC innervation and has been shown to contribute to the effects of contrast-based saliency on pupil dilation (Wang et al., 2012, 2014; Edwards et al., 1979). The anterior cingulate cortex (ACC) is a primary source of cortical input to the LC, receives projections from the LC, and has neural activity that encodes conflict- and surprise-related signals that can also be reflected in pupil diameter (Aston-Jones and Cohen, 2005; Ebitz and Platt, 2015; Porrino and Goldman-Rakic, 1982; Hayden et al., 2011). The posterior cingulate cortex (CGp) is strongly interconnected with the ACC and receives LC input (Levitt and Moore, 1978; Heilbronner and Haber, 2014).

We assessed relationships between pupil diameter and neural activity from each brain region in several ways. First, we directly compared pupil diameter and single-unit spiking activity during

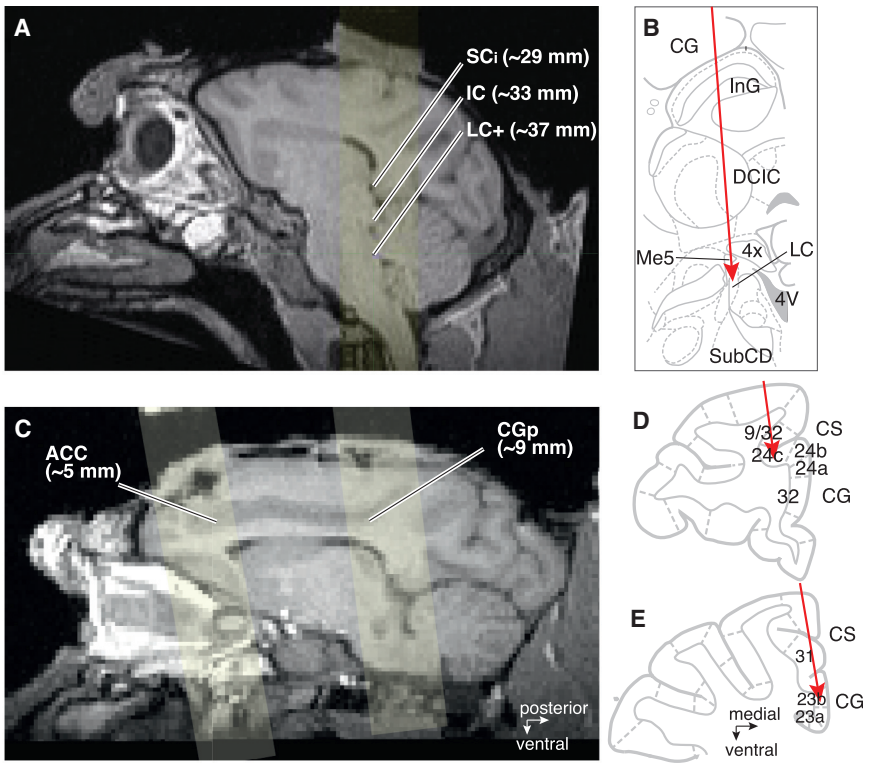

Figure 1. Recording Site Locations

(A) Approximately sagittal MRI section for monkey Ci showing estimated recording site locations in SC_i, IC, and LC+, along with the approximate depth from the cortical surface along the electrode tract.

(B) Schematic of a coronal section of the macaque brain showing structures typically encountered along our electrode tracts (adapted from Paxinos et al., 2008; Plate 90, Interaural 0.3, bregma 21.60; see also Kalwani et al., 2014, Figure 3).

(C) Approximately sagittal MRI section for monkey Sp showing estimated recording sites in ACC and CGp, along with the approximate depth from the cortical surface along the electrode tract.

(D and E) Schematic of a coronal section of the macaque brain showing structures typically encountered along our electrode tracts to ACC (D; adapted from Paxinos et al., 2008; Plate 16, Interaural 33.60, bregma 11.70) or CGp (E; adapted from Paxinos et al., 2008; Plate 89, Interaural 0.75, bregma −21.15). Lightly shaded yellow regions in (A) and (C) correspond to the three-dimensional projections of the recording cylinder (Kalwani et al., 2009).

Arrows in (B), (D), and (E) show approximate electrode tracts. CG, cingulate gyrus; CS, cingulate sulcus; DCIC, dorsal complex of the IC; InG, intermediate gray of the SC; Me5, mesencephalic 5 tract; SubCD, dorsal subcoeruleus; 4v, fourth ventricle; 4x, trochlear decussation; 9/32 and 24c, ACC (dorsal); 32, 24a, and 24b, ACC (ventral); 23a, 23b, and 31, CGp.

passive fixation, which allowed us to identify relationships that were not dependent on external events that might separately affect pupil diameter and neural activity. We assessed these relationships on different timescales, including sustained or baseline periods lasting several seconds and shorter periods that could be related to the timing of single spikes. Second, we analyzed pupil-related differences in local field potentials (LFPs), which can reflect neuromodulatory influences like that provided by the LC-NE system (Bari and Aston-Jones, 2013; Lee and Dan, 2012). Third, we tested whether changes in pupil diameter and in spiking activity evoked by repeated presentations of the same arousing sound stimulus at unpredictable times covary on a trial-by-trial basis (i.e., a test of noise correlations) to complement and extend recent findings that different task conditions can, on average, drive co-variations in pupil diameter and LC activity (i.e., a measure of signal correlations) (Varazzani et al., 2015). Fourth, for LC+, IC, and SC_i, we used electrical microstimulation to probe how reliably pupil changes can be elicited by manipulating local neural activity. The results indicate that pupil diameter can be a reliable marker of activation of LC+ but that this relationship is not specific to the LC+. Pupil diameter and neural activity are also reliably linked in the IC, SC_i, and, to a lesser extent, cingulate cortex, possibly reflecting widespread, coordinating influences of the LC-NE system.

RESULTS

We related pupil diameter to neural activity measured separately in each of five brain regions (LC+: n = 43 single units isolated from 33 multi-unit/LFP recording sites in monkey Oz and 61/52 in monkey Ci; IC: 64/68 in Oz and 66/78 in Ci; plus smaller sample sizes for the remaining three regions, which can affect the reliability of the results: SC_i: 14/12 in Oz and 21/20 sites in Ci; ACC: 40/43 in monkey Sp and 6/7 in monkey At; and CGp: 25/13 in Sp and 10/14 in monkey Ch; Figure 1) while they maintained steady fixation (60 cm viewing distance) under dim, steady lighting conditions (luminance at the monkeys' eyes: 3.5 cd/m^2; luminance of the fixation spot measured on the display: 125 cd/m^2).

During stable, near fixation, pupil diameter tended to vary both across and within trials (Figures 2A and 2B). In our monkeys, these pupil fluctuations were quasi-periodic, with oscillations at ~1–3 Hz evident on individual trials but with a periodicity and amplitude that varied considerably from cycle to cycle (Figure 2B). Therefore, we characterized each cycle individually, in terms of the duration and magnitude of dilations and constrictions defined by zero-crossings of the first derivative of pupil diameter. These durations were broadly distributed less than ~1,000 ms, with slightly longer dilations (overall median = 329 ms; interquartile range [IQR] = 230–471 ms) than constrictions (288 ms [IQR = 211–395 ms]; Wilcoxon rank-sum test, $p < 0.01$) that were roughly consistent across the five monkeys (median dilations lasted between 290 and 351 ms, and median constrictions lasted between 254 and 319 ms for each of the five monkeys; Figure 2C). The magnitude of these fluctuations depended on the baseline value of pupil diameter at the time of the fluctuation, likely reflecting asymmetries in the mechanical

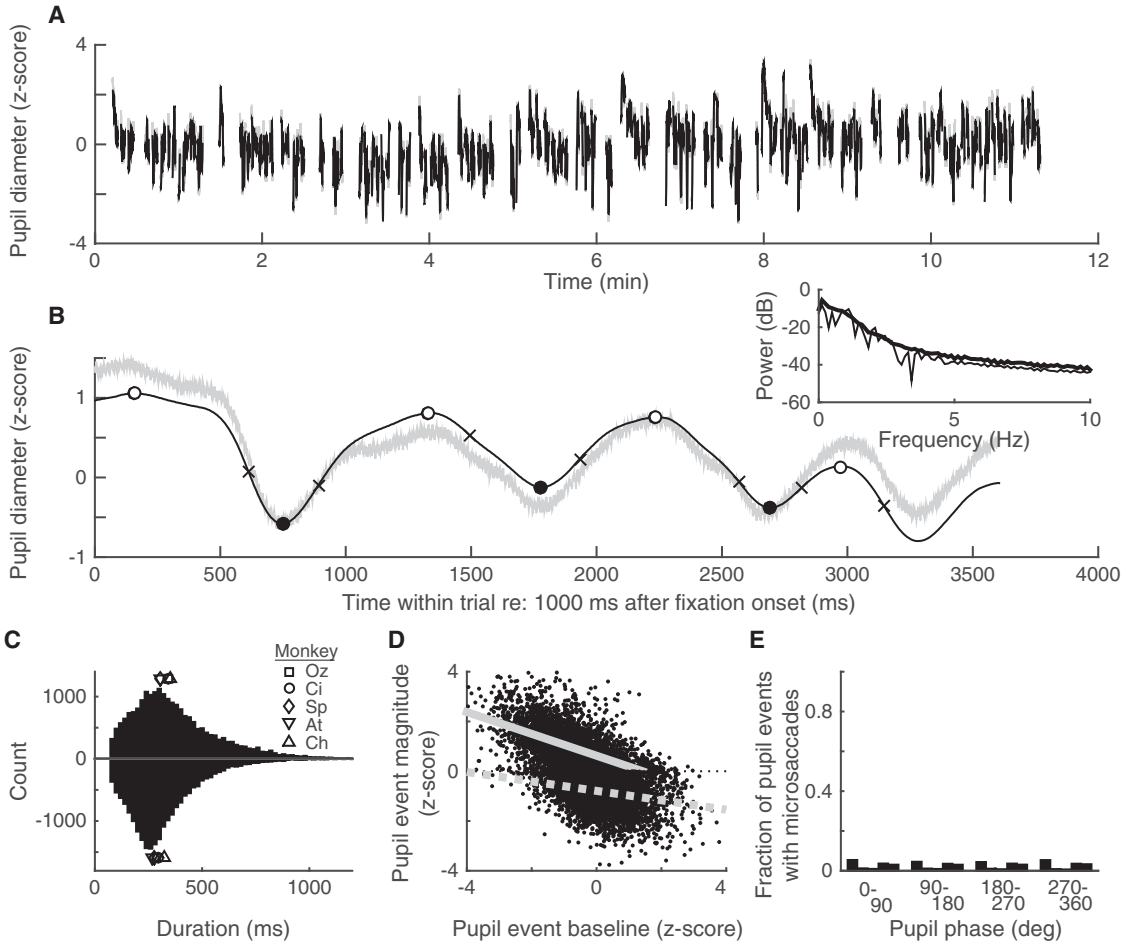

Figure 2. Measuring Pupil Diameter

(A) Pupil diameter measured during one recording session (monkey Oz). Only stable fixation epochs used for further analyses are shown; thus, data breaks represent unstable fixations and inter-trial intervals.

(B) Single-trial raw (gray) and smoothed and standardized (black) pupil traces during stable fixation. Open and closed circles indicate local maxima and minima, respectively, which define pupil "events." Crosses indicate the peak slope of the pupil signal between extrema. Inset shows pupil power spectrum (thin line is the example trial, and thick line is trial mean for this session).

(C) Distribution of pupil event durations for all monkeys and all sessions. Dilation times (intervals between each local minimum and the subsequent maximum) are shown above the x axis, whereas constriction times (intervals between each local maximum and the subsequent minimum) are shown below it. Median values for each of the five monkeys are shown as different (overlapping) symbols, as indicated.

(D) Per-cycle pupil event baseline versus fluctuation magnitude, measured for one representative monkey. Gray lines show linear regressions for dilations (solid) and constrictions (dashed).

(E) Proportion of pupil events with microsaccades, plotted as a function of the phase of the pupil event in which it occurred (five bars per bin represent the five monkeys, ordered as in the legend in C). For all five monkeys, the distributions were uniform with respect to phase (Rayleigh test, $p > 0.05$).

properties of the iris musculature (Loewenfeld and Newsome, 1971): larger transient dilations occurred when the pupil was more constricted, and, to a lesser extent, larger transient constrictions occurred when the pupil was more dilated (Figure 2D). These fluctuations were not consistently associated with small eye movements (Martinez-Conde et al., 2013; Krekelberg, 2011), which occurred less frequently and without a consistent phase relationship with respect to the fluctuations in pupil diameter (Figure 2E). The pupil fluctuations also did not appear to reflect the monkeys' heart rate, which was typically the range of ~140–150 beats per minute (i.e., a full period of ~400–430 ms, which was substantially shorter than the median full period of pupil fluctuations). Thus, these fluctuations appear to be consistent with previous reports of pupil noise (Stanten and Stark, 1966), spontaneous pupil oscillations (Warga et al., 2009), or pupillary unrest (Loewenfeld, 1999; Bokoch et al., 2015). These phenomena are not caused by similar microfluctuations in accommodation that can also occur during near fixation (Alpern et al., 1961; Stark and Atchison, 1997; Hunter et al., 2000) but, instead, are thought to reflect variability in the firing patterns of brainstem neurons that control pupil diameter (Loewenfeld, 1999; Bokoch et al., 2015).

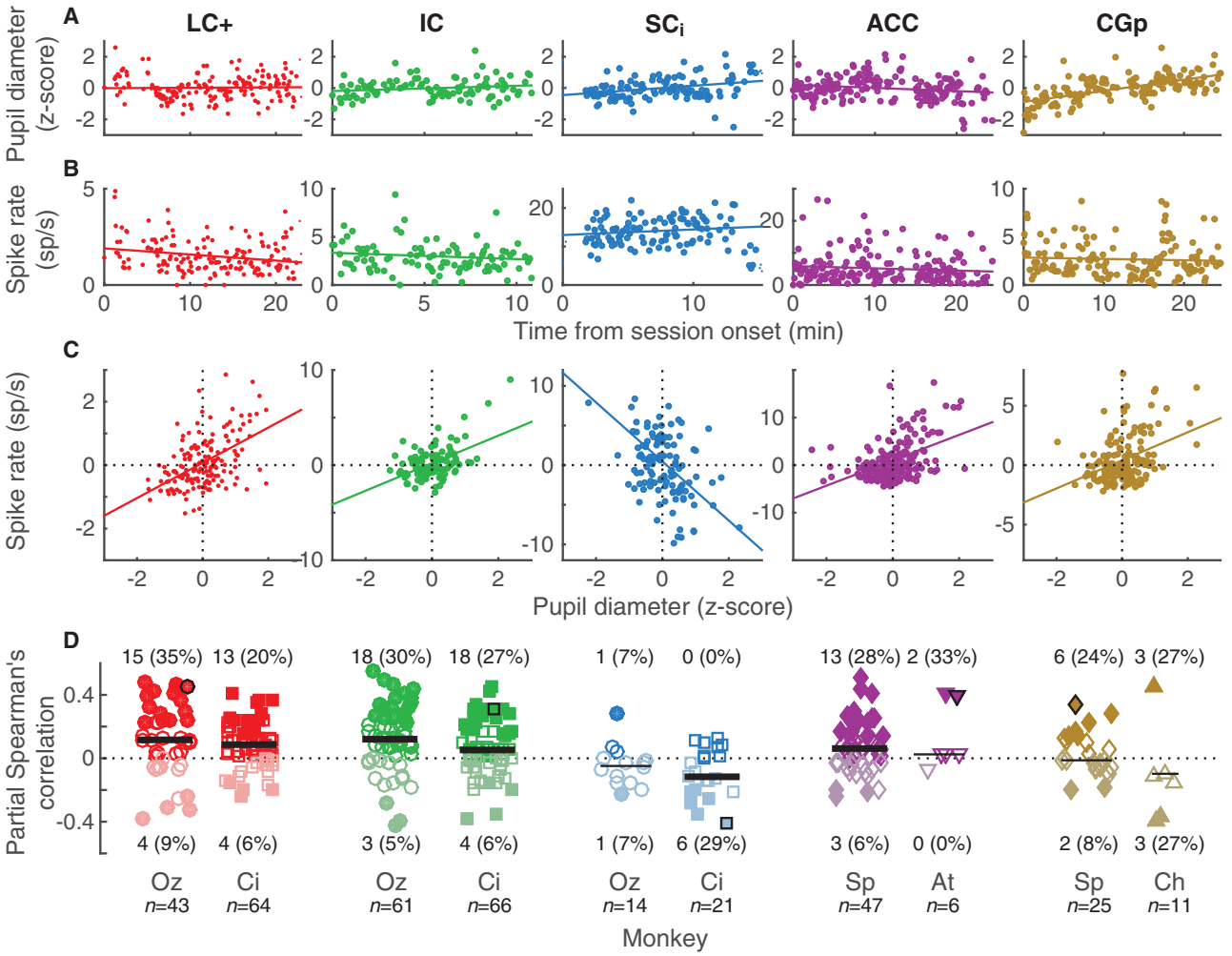

Figure 3. Trial-by-Trial Associations between Mean Pupil Diameter and Spike Rate for Each Brain Region, as Indicated by Columns

(A–C) Example sessions. Per-trial mean pupil diameter (A) and spike rate (B) are each plotted as a function of the time of the beginning of stable fixation in the given trial, with respect to the beginning of the session. Lines are linear fits; (C) shows residuals to these fits. The line is a linear fit to the paired residuals, representing the partial correlation between pupil diameter and spike rate, accounting for linear drifts of each variable as a function of time within the session.

(D) Distributions of Spearman's partial correlations (ρ) between trial-by-trial pupil diameter and spike rate, accounting for time within the session, for each session from each monkey and each brain region, as indicated. Darker/lighter symbols indicate $\rho > 0/\rho < 0$. Filled symbols indicate H_0: $\rho = 0$, $p < 0.05$. Counts (percentages) of significant positive/negative effects are shown for each monkey (per-monkey percentages for positive or negative effects were indistinguishable between LC+ and IC but were different for SCi, including fewer positive effects for both monkeys and more negative effects for monkey Ci; chi-square test, $p < 0.05$). Black symbols indicate the example sessions above. Scatter along the abscissa is arbitrary, for readability. Horizontal lines are medians; thick lines indicate H_0: median = 0, Wilcoxon rank-sum test, $p < 0.05$.

Relationship between Pupil Diameter and Spiking Activity during Passive Fixation

During passive fixation, spontaneous fluctuations in pupil diameter had consistent relationships to concurrently measured spiking activity on relatively long (trial-by-trial) and short (with respect to individual spikes) timescales. As detailed in the following text, these relationships were particularly strong for activity measured in LC+ and IC but were also evident for certain sites in SC_i, ACC, and CGp.

As has been reported previously for one LC site (Aston-Jones and Cohen, 2005), we found numerous compelling examples of correlations between trial-by-trial average values of pupil diameter and spiking activity from select sites in several brain regions. An example LC+ session is shown in Figures 3A–3C. Trials with relatively dilated (constricted) pupils tended to correspond to relatively high (low) mean spike rates, even after accounting for overall linear trends of both measurements over the course of the session (partial Spearman's correlation coefficient = 0.45, $p < 0.001$). Similar examples are shown for IC, ACC, and CGp (Figures 3A–3C). We also found some sites with negative correlations between pupil diameter and spike rate, particularly in SC_i (an example session is shown in Figures 3A–3C).

These trial-by-trial relationships between pupil diameter and spike rates were statistically reliable across the populations of

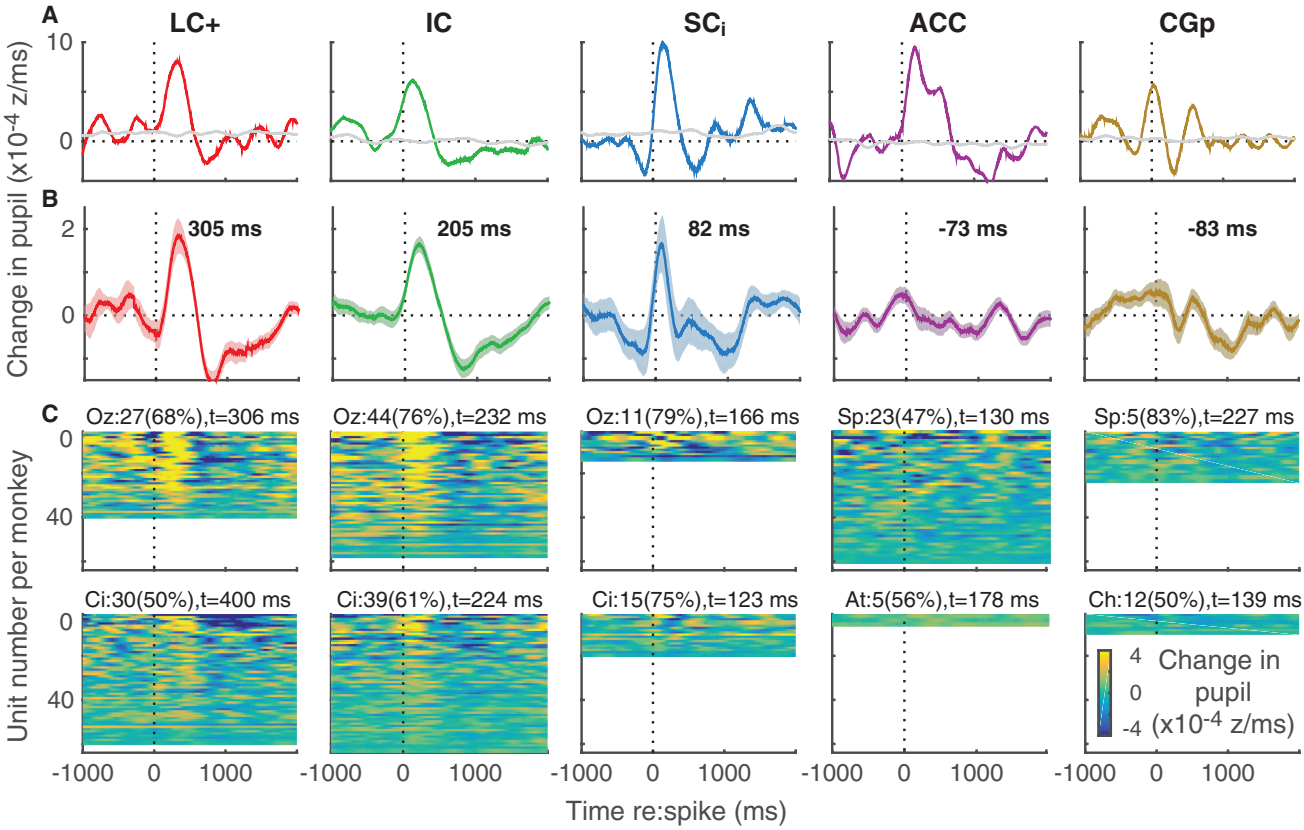

Figure 4. Spike-Triggered Changes in Pupil Diameter for Each Brain Region, as Indicated by Columns

(A) Example units. Colored lines are mean values computed from all spikes recorded during stable fixation in the given session. Gray lines are values computed after shuffling pupil diameter relative to spiking activity on a trial-by-trial basis.

(B) Mean ± SEM spike-triggered changes in pupil diameter computed from the mean, real − shuffled values computed for each recorded unit from the two monkeys. The time of the maximum value is shown; bold indicates H_0: the value at that time = 0, $p < 0.05$, bootstrapped from the mean ± SEM values computed per unit for the given time bin.

(C) Mean spike-triggered changes in pupil diameter for all recorded single units, sorted by modulation depth per monkey (top rows show units with the biggest difference between the minimum and maximum values). Text indicates the count (percentage) of sites for each monkey with a reliable peak (defined as ≥75 consecutive bins with at least one bin between 100 ms before and 700 ms after the spike for which the real − shuffled value was significantly > 0, Mann-Whitney test, $p < 0.05$) and the median time of the reliable peaks. Per-monkey percentages were indistinguishable between LC+, IC, and SC_i (chi-square test, $p \geq 0.05$). All analyses used 250-ms time bins stepped in 10-ms intervals.

units we recorded in LC+ and IC but not SC_i, ACC, or CGp. For LC+ and IC, the median correlation coefficient across individual units for each monkey was >0 (Wilcoxon rank-sum test, $p < 0.004$ in all four cases) and did not differ for the two brain regions ($p > 0.05$ for each monkey). Moreover, similar proportions of individual units from these regions showed significant, positive correlations (Figure 3D). ACC units also had a tendency for such positive effects, but the median correlation coefficient was significantly >0 ($p < 0.05$) for only one monkey. For SC_i and CGp, the effects were smaller and more mixed, with more negative effects in SC_i (Figure 3D).

We found more reliable relationships between pupil diameter and neuronal activity in all five brain regions by analyzing these relationships on finer timescales. Figure 4 shows analyses of spike-triggered changes in pupil diameter; that is, the extent to which individual spikes were aligned in time with the first derivative of pupil diameter as a function of time. An example LC+ unit is shown in Figure 4A. For this unit, spikes occurring during fixation tended to be followed immediately by a brief dilation, with the peak positive change in pupil diameter occurring 310 ms after the spike, then constriction, with the peak negative change in pupil diameter occurring 750 ms after the spike. These positive and negative peaks were both distinguishable from random relationships between the measured spikes and pupil data obtained at different times (i.e., by shuffling the trial-by-trial spike and pupil data relative to each other; gray lines in Figure 4A). We found compelling examples of spike-triggered pupil effects in all five brain regions, each of which included a reliable dilation and then constriction occurring, on average, around or following the time of each spike (Figure 4A).

Subsets of neurons recorded in each brain region and from each monkey showed these kinds of reliable relationships between individual spikes and changes in pupil diameter. Population average spike-triggered changes in pupil diameter from

each brain region are shown in Figure 4B, and data from all recorded units, separated by monkey, are shown in Figure 4C. These plots indicate qualitatively similar patterns of effects across many sites, particularly those in LC+, IC, and SC_i, with transient dilations and then constrictions following spikes. More quantitatively, 47%–83% of sites in a given brain region and monkey showed statistically reliable differences between real and shuffled spike-triggered changes in pupil diameter (Figure 4C). These differences occurred in relatively restricted time windows around the time of the spike. The magnitudes of these peak values, reflecting average maximal changes in pupil diameter around the time of each spike, did not covary with the magnitudes of trial-by-trial correlations between pupil diameter and spiking activity, reflecting the relationship between average pupil diameter and average spike rate over several seconds (see Figure 3), from the same recording sites (H_0: Spearman's correlation coefficient = 0, $p > 0.05$ for each monkey and brain region). This result implies that pupil-spike relationships can take different forms over different timescales.

In addition to these rough similarities, there were differences in the timing of spike-triggered changes in pupil diameter across the five brain regions. The timing of the peaks of these curves, computed per brain region and per monkey, are shown for the population average traces in Figure 4B and computed from individual sessions with reliable peaks for each monkey in Figure 4C. In both cases, there was a progression of the peak times for data obtained across sites in the same monkeys (LC+, IC, and SC_i), with the longest lag between the spike and the dilation-related peak occurring in LC+, then a delay to IC and, finally, SC_i (an ANOVA with monkey and these three brain regions as factors had a main effect of brain region, $p = 0.03$). The effects in cortex, measured in separate monkeys and, thus, not necessarily directly comparable to the subcortical results, did not, on average, have such clear peaks, reflecting less consistent timing across recording sites, even in the same brain region of a given monkey (Figures 4B and 4C).

Complementary to these features of spike-triggered pupil measurements, there were notable patterns of pupil-triggered spike rates from all five brain regions (Figure 5). We calculated peri-event time histograms (PETHs) relative to pupil dilation or constriction events (i.e., the times of the maximum increase or decrease in pupil diameter, respectively, as a function of time for each quasi-periodic half-cycle, as shown in Figure 2B). Example units from all five brain regions showed similar pupil-dependent patterns in the rasters and associated PETHs: a transient increase in spiking preceding large dilation events (dark lines in Figure 5B) and either little change or a transient decrease in spiking preceding large constriction events (light lines in Figure 5B).

To visualize and quantify these effects, we computed, for each single unit, the mean difference in pupil-event-aligned spiking activity for large dilations versus large constrictions, as in the examples in Figures 5A and 5B. Thus, positive (or negative) values of this difference indicate higher (or lower) spike rates in the given time bin relative to dilations versus constrictions. Population averages from each brain region are shown in Figure 5C, and data from individual recording sites, separated by monkey, are shown in Figure 5D. The biggest and most consistent pupil-related modulations were evident in LC+ and IC. In these regions, a peak positive modulation occurred, on average, in a relatively restricted time frame just prior to the pupil event. The timing of this peak progressed systematically across the brainstem sites, from LC+ to IC to SC_i, relative to the pupil event (Figures 5C and 5D). For the cortical sites, similar proportions of units as for the subcortical sites showed these modulations (30%–60%), but partly because the timing of these modulations varied considerably across units, the average effects were smaller in ACC and CGp (Figures 5C and 5D).

Relationship between Pupil Diameter and LFPs during Passive Fixation

LFPs can represent aspects of neuromodulatory influence and network function that are different from spiking activity (Bari and Aston-Jones, 2013; Lee and Dan, 2012). Therefore, we also assessed relationships between spontaneous fluctuations in pupil diameter measured during passive fixation and LFPs. Pupil-linked effects were evident in the difference between dilation- and constriction-linked raw LFPs aligned to the time of pupil events. Example sites from each brain region showed a prominent negative trough preceding the pupil event, corresponding to more a more negative LFP value preceding dilations versus constrictions (Figure 6A). This negative peak preceding the pupil event was evident in the population average traces, particularly for the brainstem sites (Figure 6B), and many traces from individual sites from each brain region (Figure 6C). As for the spike-pupil analyses, the timing of this peak varied systematically across the brainstem sites, occurring earliest in LC+, then IC, then SC_i. Across monkeys, the brainstem sites showed larger proportions of neurons with reliable effects (63%–100%) compared with cortical sites (14%–61%).

Because different frequency bands of the LFP can reflect different aspects of network function (von Stein and Sarnthein, 2000; Kopell et al., 2000; Donner and Siegel, 2011), we also assessed band-specific differences relative to pupil events (dilation versus constriction). We found prominent effects in LFP power in both low (<30 Hz) and gamma (30–100 Hz) frequency bands that differed for the different brain regions tested (Figure 6D). For the brainstem sites, the peak effects occurred, on average, < 500 ms before the associated pupil event, but primarily for the gamma band in LC+, both bands in IC, and the low-frequency band in SC_i. For the cortical sites, the effects were more mixed, with both ACC and CGp showing some early enhancement in the gamma band but little pupil-dependent structure just prior to the pupil events.

Relationship between Pupil Diameter and Neural Activity in Response to Startling Events

To examine the relationship between pupil diameter and neural activity in the context of not just internal (spontaneous) fluctuations but also external events that can cause changes in arousal, we played a brief, loud, startling tone during randomly chosen trials. For all monkeys, the tone caused a transient dilation of the pupil (Figure 7A). We found that areas LC+, IC, and ACC also exhibited consistent, transient neuronal responses to the tone in each of two monkeys (Figure 7B). In contrast, the tone evoked

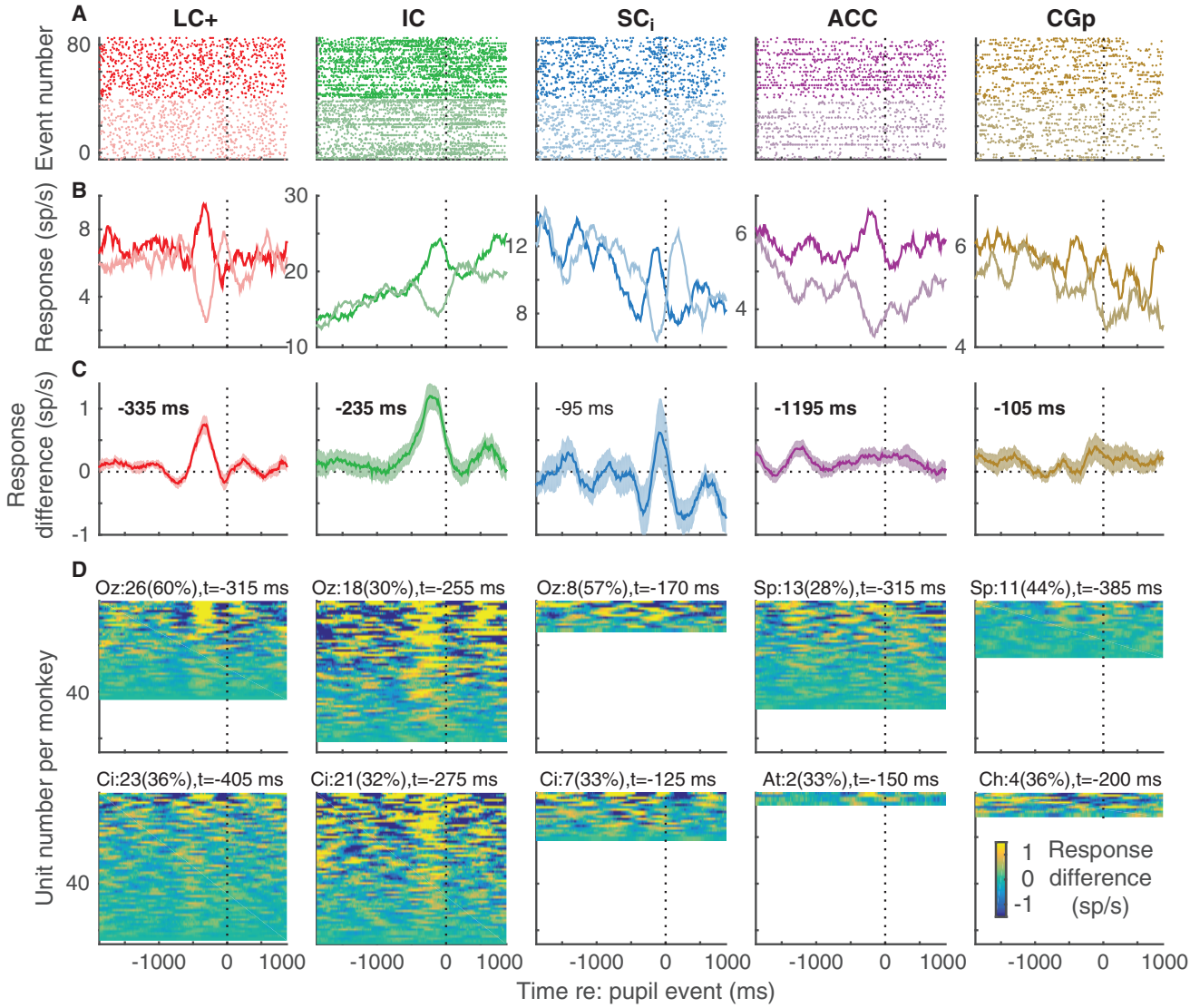

Figure 5. Spike PETHs Aligned to Pupil Events for Each Brain Region, as Indicated by Columns

(A and B) Example units. Light/dark lines show rasters (A, showing 40 randomly selected trials for each condition for presentation clarity) and PETHs (B) for large dilation/constriction events (upper/lower 25th percentile slopes; see Figure 2B), aligned to the time of the event. sp/s, spikes per second.

(C) Mean ± SEM difference in dilation- versus constriction-aligned PETHs computed for each recorded unit from the two monkeys. The time of the maximum value is shown in each panel; bold indicates H_0: the value at that time = 0, $p < 0.05$, bootstrapped from the mean ± SEM values computed per unit for the given time bin.

(D) Mean difference in dilation- versus constriction-aligned PETHs computed for all recorded single units, sorted by modulation depth per monkey (top rows show units with the biggest difference between the maximum and minimum values). Text indicates the count (percentage) of sites for each monkey with a reliable peak (defined as ≥ 7 consecutive bins with at least one bin between 1,000 ms before and 100 ms after the pupil event for which the dilation-aligned − constriction-aligned value was significantly > 0, Mann-Whitney $p < 0.05$) and the median time of the reliable peaks. Per-monkey percentages were indistinguishable between LC+, IC, and SC_i (chi-square test, $p \geq 0.05$) except for monkey Oz, LC+ versus IC. All analyses used 250-ms time bins stepped in 10-ms intervals.

consistent responses in the CGp of only one of two monkeys and did not evoke consistent responses in the SC_i of either of the two monkeys (Figure 7B). On a trial-by-trial basis, there was a weak but reliable relationship between the magnitudes of the tone-aligned neural and pupil responses only for LC+, consistent with a common driving input that has more direct effects on LC+ than the other brain regions tested (Nieuwenhuis et al., 2011) (Figure 7C).

Relationship between Pupil Diameter and Electrical Microstimulation

We used electrical microstimulation to test whether manipulation of neuronal activity at a given site in the LC+, IC, or SC_i could evoke changes pupil diameter. We found sites in each of these brain regions where microstimulation reliably evoked transient increases in pupil diameter within ~1,000 ms of microstimulation onset (Figure 8A). Across the population of tested sites,

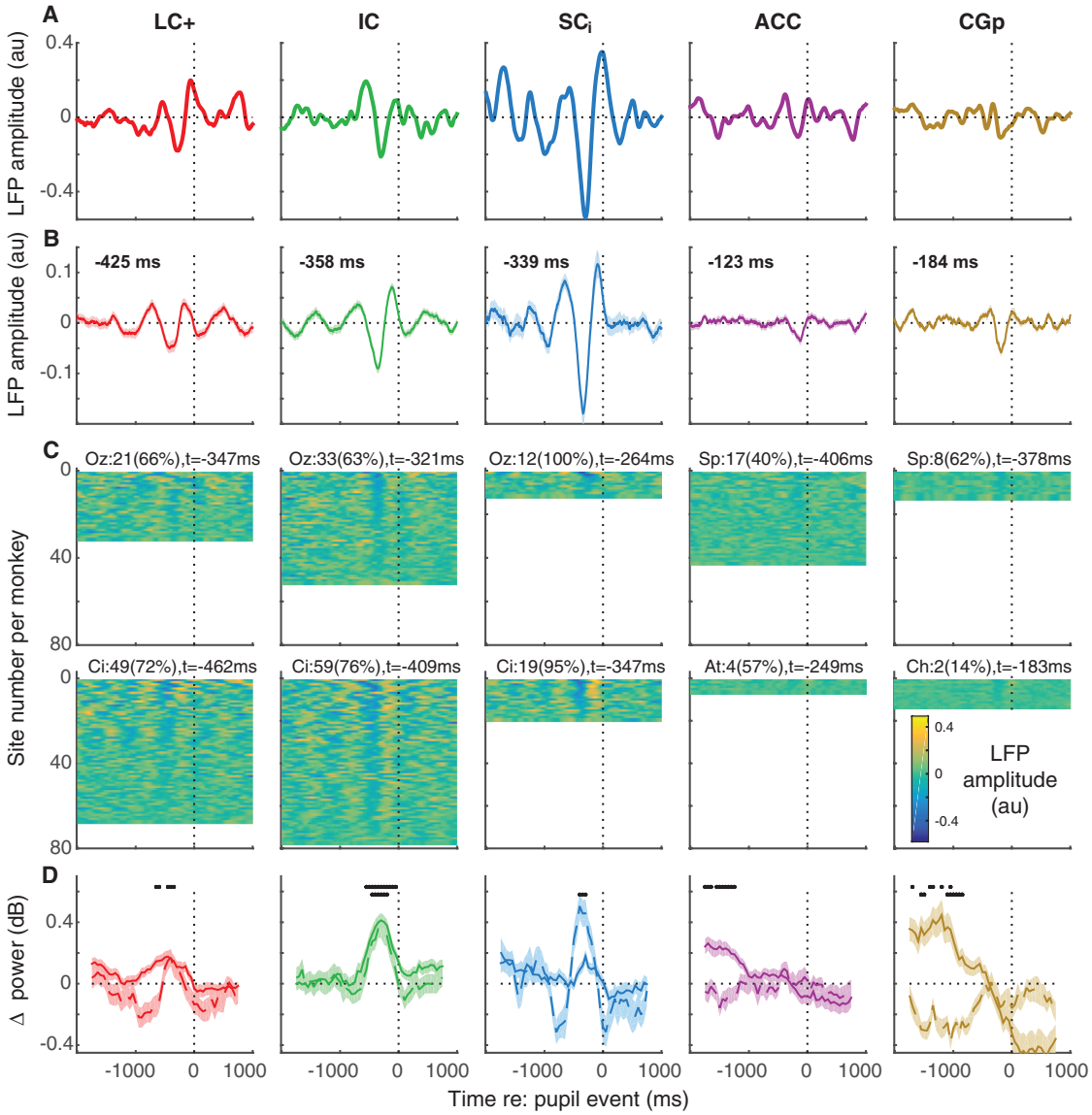

Figure 6. Pupil-Related Differences in LFP Time Course and Power Spectrum for Each Brain Region, as Indicated by Columns

(A) Differences in time-series LFPs aligned to large pupil events (dilate − constrict) for example recording sites.

(B) Mean ± SEM differences in time-series LFPs aligned to large pupil events computed for each recorded site from the two monkeys. The time of the minimum value from the mean curve is shown; bold indicates H_0: the value at that time = 0, $p < 0.05$, bootstrapped from the mean ± SEM values computed per site for the given time bin.

(C) Mean differences in time-series LFPs aligned to large pupil events computed for all recording sites, sorted by modulation depth per monkey (top rows show units with the biggest difference between dilation- and constriction-linked values). Text indicates the count (percentage) of sites for each monkey with a reliable trough (defined as at least one 75 ms window in the 1,000 ms preceding the pupil event with values that were significantly < 0; Wilcoxon rank-sum test, $p < 0.05$) and the median time of the reliable troughs.

(D) Difference (dilate − constrict) in LFP power spectra aligned to pupil events for low (<30 Hz, dashed line) and gamma (30–100 Hz) frequency bands. Black dots indicate H_0: binned value = 0, Mann-Whitney test, $p < 0.05$, corrected for multiple comparisons (upper row: gamma band; lower row: low-frequency band). All analyses used 500-ms time bins stepped in 50-ms intervals.

the effects were most consistent in LC+ (Figure 8B). There, microstimulation evoked changes in pupil diameter at all tested sites (n = 12), and, across sites, the time of the maximum evoked change in pupil diameter had mean values (per site) of 458–563 ms following microstimulation onset. In IC, the effects were slightly more variable. There, microstimulation evoked changes in pupil diameter at 12 out of 18 sites, and the time of the maximum change was 253–653 ms following microstimulation onset. Microstimulation in SC_i yielded reliable changes in pupil diameter from three of ten tested sites, as has been

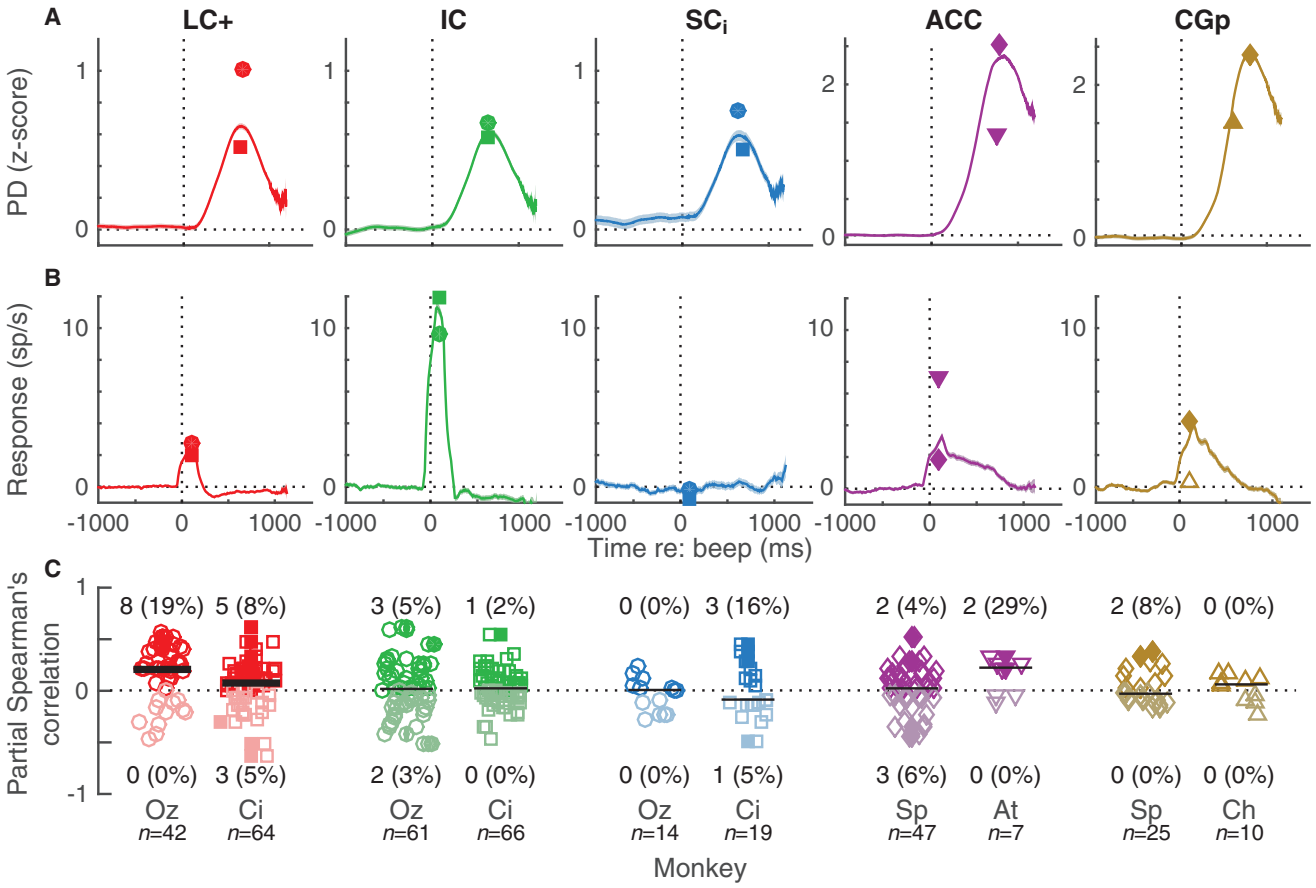

Figure 7. Responses to Startling Events for Each Brain Region, as Indicated by Columns

(A) Transient pupil dilations (PD) evoked by unexpected auditory events ("beeps"). Lines/ribbons indicate mean ± SEM across all beep trials from both monkeys. Symbols are maximum values per monkey.

(B) Spiking responses to unexpected auditory events, measured in 200-ms time bins stepped in 10-ms intervals. Lines/ribbons indicate mean ± SEM across all beep trials from both monkeys. Symbols are maximum values per monkey. Filled symbols indicate H0: maximum = 0, Mann-Whitney test, $p < 0.05$.

(C) Population summary. Spearman's partial correlation, ρ, between spiking (spike rate, 0–200 ms following beep onset minus baseline spike rate measured during fixation prior to beep onset) and pupil (maximum change in pupil diameter 0–800 ms following beep onset) responses, accounting for the effects of baseline pupil diameter on both variables. Darker/lighter symbols indicate $\rho > 0/\rho < 0$. Filled symbols indicate H_0: $\rho = 0$, $p < 0.05$. Counts (percentages) of significant positive/negative effects are shown for each monkey (for monkey Oz, the percentages for positive effects were significantly different for LC versus IC or SC_i; chi-square test, $p < 0.05$). Scatter along the abscissa is arbitrary, for readability. Horizontal lines are medians; thick line indicates H_0: median = 0, Wilcoxon rank-sum test, $p < 0.05$.

reported previously (Wang et al., 2012). The timing of these effects were more variable than for LC+ or IC, with the time of the maximum change occurring 388–813 ms following microstimulation onset.

DISCUSSION

The goal of this study was to characterize relationships between non-luminance-mediated changes in pupil diameter and neural activity. We targeted the LC (plus the adjacent subcoeruleus, which is difficult to distinguish from the LC using our recording techniques) (Kalwani et al., 2014) because of its previously proposed links to pupil diameter (Nassar et al., 2012; Nieuwenhuis et al., 2011; Varazzani et al., 2015; Phillips et al., 2000; Hou et al., 2005; Beatty, 1982a, 1982b; Richer and Beatty, 1987; Einhäuser et al., 2008; Gilzenrat et al., 2010; Morad et al., 2000; Aston-Jones and Cohen, 2005; Murphy et al., 2011, 2014). We supported and extended those findings by showing, for the first time, that the activity of subsets of LC+ neurons is related to subsequent changes in pupil diameter during stable, near fixation under several conditions: (1) trial-by-trial associations between average pupil diameter and concurrent, tonic LC+ activation; (2) changes in spiking and LFP activity that occur just prior to pupil dilations; (3) trial-by-trial associations between the magnitude of pupil and LC+ neural responses evoked by unexpected presentations of the same auditory stimulus; and (4) evoked changes in pupil diameter via electrical microstimulation in the LC+. In general, we found that LC+ activity was higher just preceding pupil dilations versus constrictions, implying that the pupil changes do not cause changes in LC+ activation

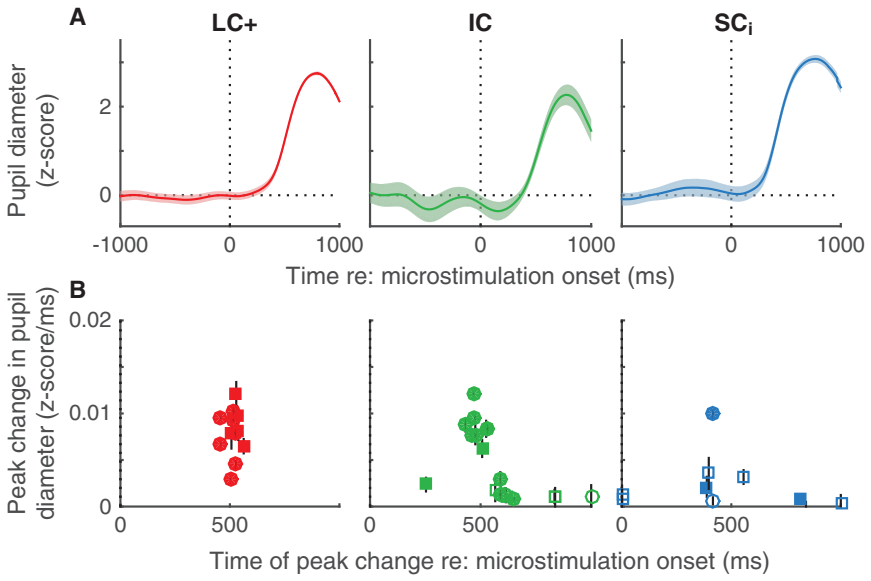

Figure 8. Effects of Electrical Microstimulation in LC+, IC, and SC_i, in Columns, on Pupil Diameter

(A) Pupil diameter aligned to the time of microstimulation onset. Lines and ribbons are mean ± SEM across all microstimulation trials from all sessions.

(B) Summary of microstimulation effects. Symbols and error bars indicate mean ± SEM peak change in pupil diameter <800 ms following microstimulation onset from individual trials in a given session, plotted as a function of the time of the peak. Closed symbols indicate H_0: peak change = 0, Wilcoxon rank-sum test, $p < 0.05$.

(e.g., via associated changes in visual input to the brain) but rather that both the pupil and LC+ may reflect underlying changes in arousal that can occur on fine timescales.

We also showed that relationships between neural activity and pupil diameter are not unique to the LC+ but, instead, can also be found for several other brain regions, including the IC, SC_i, ACC, and CGp. Substantial fractions of recorded units from each brain region exhibited spiking and LFP activity that was modulated in association with changes in pupil diameter, consistent with previous reports for numerous cortical regions in humans, non-human primates, and rodents performing various tasks (Vinck et al., 2015; Reimer et al., 2014; Ebitz and Platt, 2015; Eldar et al., 2013; McGinley et al., 2015). The effects in IC were particularly robust and, as for LC+ and SC_i (Wang et al., 2012), could be elicited via electrical microstimulation. These widespread effects suggest that, at least during stable fixation and in the absence of complex task-related processing, neural activity throughout many cortical and subcortical structures can be aligned in time with fluctuations in pupil diameter.

What mechanism can explain these phenomena? Constriction and dilation of the pupil is controlled by a balance of parasympathetic and sympathetic components, including inhibition of parasympathetic-controlled, tonic activation of the sphincter pupillae by the Edinger-Westphal nucleus and direct sympathetic activation of the dilator muscles (Loewenfeld, 1999). This balance is controlled by other circuits that give rise to pupil changes in response to changes in light, fixation, or other complex functions, including arousal, orienting, and cognition (Andreassi, 2000). There are no known anatomical pathways that could subserve a direct influence of the LC+ on these autonomic circuits in primates (Nieuwenhuis et al., 2011). Instead, the relationship between LC+ activation and pupil diameter likely involves sources of common input to the two systems.

For external events that drive transient LC responses, this common driving force has been proposed to involve the paragigantocellularis nucleus (PGi) of the ventral medulla, which receives widespread cortical and subcortical inputs and projects to both the Edinger-Westphal nucleus and the LC (Vogt et al., 2008; Breen et al., 1983; Nieuwenhuis et al., 2011). The PGi can mediate evoked, transient LC responses under at least some conditions (Hajós and Engberg, 1990; Ennis and Aston-Jones, 1988; Ennis et al., 1992; Chiang and Aston-Jones, 1993; Van Bockstaele et al., 1998). Thus, a circuit involving the PGi that co-modulates the LC and the sympathetic nervous system is consistent with our findings related to external event (unexpected sound)-related responses, which showed trial-by-trial relationships between neural- and pupil-response magnitude only for LC+. This circuit might also account for task-driven pupil changes previously reported to covary with activation of neurons in LC but not dopaminergic neurons in the substantia nigra pars compacta, which is not known to receive substantial PGi inputs (Varazzani et al., 2015; Lee and Tepper, 2009; Bezard et al., 1997).

The PGi might also have contributed to our LC+ microstimulation effects. According to this idea, LC+ microstimulation causes direct, antidromic activation of PGi, which, in turn, affects the pupil in a consistent manner. The consistent LC+ effects might also reflect a relatively higher level of homogeneity in the functional properties of LC+ neurons around the sites of microstimulation, as compared to IC and SC_i, although several recent studies have begun to challenge the long-held notion of LC as a functionally and anatomically uniform structure (Chandler et al., 2014; Schwarz et al., 2015).

Another, although not mutually exclusive, possibility is a circuit that is centered on the SC_i and the mesencephalic cuneiform nucleus (MCN) (Wang and Munoz, 2015). This pathway has been proposed to play a key role in changes in pupil diameter that are associated with certain aspects of cognitive processing, including attention and orienting to salient stimuli (Wang and Munoz, 2015). Cholinergic modulation of these circuits also plays a role in attentional processing and might contribute to pupil effects, although such contributions have not yet been investigated directly (Yu and Dayan, 2005; Wang et al., 2006; Mysore and Knudsen, 2013). At the very least, these circuits involving the SC_i likely contributed to our SC_i microstimulation results. They might have also contributed to the sound-driven pupil changes, which likely reflected an abrupt change in arousal

and attention. In principle, such a contribution is possible even in the absence of consistent, trial-by-trial relationships between the sound-driven SC_i and pupil responses, because those relationships measured via individual neurons are likely to be sensitive to the magnitude of correlated activity between individual SC_i neurons (Shadlen et al., 1996), which has not yet been well characterized.

For our reported relationships between pupil diameter and neural activity in LC+ and elsewhere that occurred during sustained fixation and were not explicitly driven by external events, the underlying circuits are less clear. In humans, spontaneous fluctuations in pupil diameter are suppressed by opioids, leading to the suggestion that they are driven by fluctuating inputs to the Edinger-Westphal nucleus from opioid-sensitive neurons in the periaqueductal gray (Bokoch et al., 2015). These and other circuits, possibly including the PGi, SC_i, MCN, and other brain areas that modulate autonomic control of the pupil during nominally steady-state conditions, may also contribute to co-activation of LC+ activity.

Regardless of the source of spontaneous, covarying fluctuations in LC+ activation and pupil diameter during near fixation, one important consequence is the associated, timed release of NE throughout the brain. NE release can enhance both excitatory and inhibitory effects of incoming signals on targeted neurons, thus serving as a modulator of overall neural gain (Servan-Schreiber et al., 1990; Eldar et al., 2013; Aston-Jones and Cohen, 2005; Waterhouse et al., 1980; Segal and Bloom, 1976; Dillier et al., 1978). Such changes in gain, which also might involve astrocyte networks (Paukert et al., 2014) or other neuromodulatory and circuit mechanisms (Yu and Dayan, 2005; Lee and Dan, 2012; Salinas and Sejnowski, 2001; Haider and McCormick, 2009), would, in principle, affect coordinated activity throughout the brain in relation to the pupil changes that were co-modulated with the LC+ (Eldar et al., 2013; Aston-Jones and Cohen, 2005). Thus, according to this idea, the pupil and LC+ are part of an arousal network that undergoes spontaneous fluctuations when an individual is in an attentive state but not necessarily performing an explicit task. These LC+ fluctuations, in turn, cause NE release, which results in neural activity patterns throughout many parts of the brain that are coordinated with the pupil fluctuations, an idea that merits further study.

This neuromodulatory framework could, in principle and at least qualitatively, account for some of our results. In particular, we found that pupil-related changes in LC+ activity consistently preceded those found in IC and SC_i in the same monkeys by many tens of milliseconds. Accordingly, LC+-mediated NE release could have contributed to the changes in neural activity in these other brain regions (Aston-Jones and Cohen, 2005). However, such contributions do not exclude other network mechanisms. For example, the ACC both receives projections from and sends projections to LC+ and other brainstem nuclei, and CGp and ACC are heavily interconnected (Aston-Jones and Cohen, 2005; Porrino and Goldman-Rakic, 1982). These multiple pathways may help to explain the more variable—and, in some cases, leading (Figures 4, 5, and 6)—timing of pupil-related modulations of neuronal activity in cingulate cortex relative to LC+, IC, and SC_i, which may, in part, reflect signals occurring first in cingulate and then transmitted to the LC+.

A combination of neuromodulatory and network effects may also account for our spectral results. Band-specific LFP power, which characterizes local oscillatory patterns, likely reflects network interactions (von Stein and Sarnthein, 2000; Kopell et al., 2000; Donner and Siegel, 2011). In particular, local interactions are thought to underlie gamma-band enhancements, whereas the linkage of such local processing with integrative, cognitive processes is thought to enhance lower frequency bands. In our data, all three brainstem sites showed pupil-linked modulation in both frequency ranges. However, the LC+ had a distinctive relative abundance of higher versus lower frequency band modulations, suggesting pupil-linked changes in local processing there. Such local processing may include the integration of inputs into LC+ to generate spiking output, accompanied by release of NE elsewhere in the brain. This timed NE release, possibly in tandem with other neuromodulatory systems, may contribute to links between pupil fluctuations; network activity (or cortical states); and sensory, motor, and cognitive processing (Polack et al., 2013; Reimer et al., 2014; McGinley et al., 2015; Vinck et al., 2015; Sara and Bouret, 2012; Aston-Jones and Cohen, 2005; Briand et al., 2007). More work is needed to elucidate the specific, possibly neuromodulatory, mechanisms responsible for the links between pupil changes and the neural and behavioral phenomena that have been found for a much wider range of task conditions than we addressed in the present study.

EXPERIMENTAL PROCEDURES

Five adult male rhesus monkeys (*Macaca mulatta*) were used for this study. All training, surgery, and experimental procedures were performed in accordance with the NIH's Guide for the Care and Use of Laboratory Animals and were approved by the University of Pennsylvania Institutional Animal Care and Use Committee.

Behavioral Task

The monkeys performed a fixation task. All trials began with the presentation of a central fixation point. The monkey fixated for a variable period of time (1–5 s, uniformly distributed). The trial ended when the fixation point was turned off. The monkey was rewarded with a drop of water or Kool-Aid for maintaining fixation until the end of the trial. On about 25% of randomly chosen trials, a sound (1 kHz, 0.5 s) was played over a speaker in the experimental booth (beep trials) after 1–1.5 s of fixation. The monkey was required to maintain fixation through the presentation of the sound, until the fixation point was turned off.

Pupillometry

All measurements were made in a closed booth, with the fixation point as the only source of luminance. To ensure reliable measurements of pupil diameter that were not influenced by changes in eye position (Hayes and Petrov, 2015), we included for analysis only those periods of fixation that started at least 1 s after fixation onset and did not include any saccadic events, defined as changes in eye position with a minimum distance of 0.2°, a minimum peak velocity of 0.08°/ms, a minimum instantaneous velocity of 0.04°/ms, and a minimum instantaneous acceleration of $0.005°/ms^2$. Eye position was highly stable during these epochs (Mann-Whitney test for H_0: no difference in eye position at the beginning versus the end of each fixation epoch; $p > 0.05$ for 294/306 sessions across all monkeys). The fixation intervals included for analysis had a median duration of 3,108 ms; IQR = 2,539–3,644 ms. Pupil diameter was measured monocularly in a.u. using a video-based eye-tracking system (EyeLink 1000, SR Research) sampled at 1,000 Hz. Raw pupil measurements were *Z* scored for each session (for reference, an increase in pupil diameter of 1 SD from the mean corresponded to a median increase in pupil area of 21.3% [IQR = 16.0%–28.9%] across all sessions). To remove persistent effects of the changes in eye position and luminance that can result from fixation onset, the

time-dependent, *Z* scored pupil trace from each trial was standardized by subtracting the mean, across-trial pupil trace per session, aligned to fixation onset. Finally, these standardized traces were smoothed using a 151-ms-wide boxcar filter. Pupil slope was computed as the slope of a linear fit to a 151-ms-wide running window of the smoothed, standardized pupil-diameter measurements as a function of time within a trial. Pupil events were defined as maximum positive values (dilations) and negative values (constrictions) of the slope between sequential zero-crossings of the slope separated by $\geq$75 ms. Microsaccades (Figure 2E) were defined as changes in eye position, with a minimum instantaneous velocity of 0.015°/ms and a minimum duration of 6 ms.

Electrophysiology

Monkeys Oz and Ci were each implanted with a single recording cylinder that provided access to LC+, IC, and SC_i. The detailed methodology for targeting and surgically implanting the recording cylinder and then targeting, identifying, and confirming recording sites in these three brain regions is described elsewhere for the exact sites used in this study (data for the two studies were collected in separate blocks in the same recording sessions) (Kalwani et al., 2014). Briefly, SC_i units exhibited spatial tuning on a visually guided saccade task and could elicit saccades via electrical microstimulation (Robinson, 1972; Sparks and Nelson, 1987). IC units exhibited clear responses to auditory stimuli. LC+ units, which likely came from sites in either the LC or the adjacent, NE-containing subcoeruleus nucleus (Sharma et al., 2010; Paxinos et al., 2008; Kalwani et al., 2014), had relatively long action-potential waveforms, were sensitive to arousing external stimuli (e.g., door knocking), and decreased firing when the monkey was drowsy (e.g., eyelids drooped) (Aston-Jones et al., 1994; Bouret and Sara, 2004; Bouret and Richmond, 2009). These sites were verified by using MRI and assessing the effects of systemic injection of clonidine on LC+ responses in both monkeys and by histology with electrolytic lesions and electrode-tract reconstruction in monkey Oz. Recording and microstimulation at these sites were conducted using custom-made electrodes (made from quartz-coated platinum-tungsten stock wire from Thomas Recording) and a Multichannel Acquisition Processor (Plexon).

We targeted ACC and CGp on either the left side (in monkeys Sp and Ch) or the right side (in monkey At). ACC cylinders were placed at Horsley-Clarke coordinates 33 mm anterior-posterior (AP), 8 mm lateral (L), for monkey Sp; and 43 mm AP, 8 mm L, for monkey At. The CGp cylinder for monkey Sp was placed at 0 mm AP, 5 mm L, and was tilted at an angle of 8.5° along the medial-lateral (ML) plane to point toward the midline. The CGp chamber for monkey Ch was placed at −5.3 AP, 12.2 mm L. For ACC recordings, we targeted the dorsal bank of the anterior cingulate sulcus (~4–6 mm below the cortical surface). For CGp recordings, we targeted areas 31 and 23, in the posterior cingulate gyrus (~7–11 mm below the cortical surface). Both brain regions were targeted using MRI and custom software (Kalwani et al., 2009), as well as by listening for characteristic patterns of white and gray matter during recordings. Recordings were conducted using either single-contact glass-coated tungsten electrodes (Alpha Omega) or multicontact linear electrode arrays (V-probe, Plexon).

For each brain region, we recorded and analyzed data from all stable, well-isolated units that we encountered. Neural recordings were filtered between 100 Hz and 8 kHz for spikes and between 0.7 Hz and 170 Hz for LFPs. Spikes were sorted offline. Spectral analyses of the LFP were conducted using the Chronux toolkit (Bokil et al., 2010). LFP data were preprocessed using the "rmlinesc" function (Chronux) to remove 60-Hz line noise. Spectrograms were computed using a 0.5-s moving window with a 0.05-s step size, plus 19 tapers, resulting in spectral smoothing of ±20 Hz.

Electrical microstimulation in LC+, IC, or SC_i consisted of biphasic (negative-positive) pulses, 0.3 ms long and delivered at 300 Hz via a Grass S-88 stimulator through a pair of constant-current stimulus isolation units (Grass PSIU6) that were linked together to generate the biphasic pulse. Microstimulation duration was 50, 100, or 400 ms. For LC+, microstimulation current was chosen in a range that did not evoke a visible startle response (10–30 μA). For IC, the same range was used. For SC_i, the current was set at a value just below the threshold for evoking saccades (10–90 μA). We did not find any systematic differences in the probability, magnitude, or timing of evoked changes in pupil diameter using the different values of microstimulation duration or current amplitude, so the results are combined across all values of these parameters.

Data Analysis

The magnitude of spontaneous and evoked changes in pupil diameter depends on baseline magnitude (Figure 2D). Therefore, measured associations between the magnitude of spontaneous (Figure 5) or evoked (Figure 7) changes in pupil diameter with neural activity used partial correlations that accounted for effects of baseline pupil diameter on both variables.

AUTHOR CONTRIBUTIONS

R.M.K. implemented the experimental task; S.J., Y.L., and R.M.K. collected the data; and S.J. and J.I.G. analyzed the data and wrote the paper. All authors designed the research; discussed the analyses, results, and interpretation; and revised the paper.

ACKNOWLEDGMENTS

We thank Long Ding, Takahiro Doi, and Merlin Larson for valuable comments and Jean Zweigle for expert animal care and training. This work was funded by NIH grant R21 MH-093904.

Received: August 4, 2015
Revised: October 25, 2015
Accepted: November 11, 2015
Published: December 17, 2015

REFERENCES

Alnæs, D., Sneve, M.H., Espeseth, T., Endestad, T., van de Pavert, S.H., and Laeng, B. (2014). Pupil size signals mental effort deployed during multiple object tracking and predicts brain activity in the dorsal attention network and the locus coeruleus. J. Vis. *14*, 1–20.

Alpern, M., Mason, G.L., and Jardinico, R.E. (1961). Vergence and accommodation. V. Pupil size changes associated with changes in accommodative vergence. Am. J. Ophthalmol. *52*, 762–767.

Andreassi, J.L. (2000). Pupillary response and behavior. In Psychophysiology: Human behavior and physiological response (Erlbaum), pp. 218–233.

Aston-Jones, G., and Cohen, J.D. (2005). An integrative theory of locus coeruleus-norepinephrine function: adaptive gain and optimal performance. Annu. Rev. Neurosci. *28*, 403–450.

Aston-Jones, G., Rajkowski, J., Kubiak, P., and Alexinsky, T. (1994). Locus coeruleus neurons in monkey are selectively activated by attended cues in a vigilance task. J. Neurosci. *14*, 4467–4480.

Bari, A., and Aston-Jones, G. (2013). Atomoxetine modulates spontaneous and sensory-evoked discharge of locus coeruleus noradrenergic neurons. Neuropharmacology *64*, 53–64.

Beatty, J. (1982a). Phasic not tonic pupillary responses vary with auditory vigilance performance. Psychophysiology *19*, 167–172.

Beatty, J. (1982b). Task-evoked pupillary responses, processing load, and the structure of processing resources. Psychol. Bull. *91*, 276–292.

Bezard, E., Boraud, T., Bioulac, B., and Gross, C.E. (1997). Compensatory effects of glutamatergic inputs to the substantia nigra pars compacta in experimental parkinsonism. Neuroscience *81*, 399–404.

Bokil, H., Andrews, P., Kulkarni, J.E., Mehta, S., and Mitra, P.P. (2010). Chronux: a platform for analyzing neural signals. J. Neurosci. Methods *192*, 146–151.

Bokoch, M.P., Behrends, M., Neice, A., and Larson, M.D. (2015). Fentanyl, an agonist at the mu opioid receptor, depresses pupillary unrest. Auton. Neurosci. *189*, 68–74.

Bouret, S., and Sara, S.J. (2004). Reward expectation, orientation of attention and locus coeruleus-medial frontal cortex interplay during learning. Eur. J. Neurosci. *20*, 791–802.

Bouret, S., and Richmond, B.J. (2009). Relation of locus coeruleus neurons in monkeys to Pavlovian and operant behaviors. J. Neurophysiol. *101*, 898–911.

Breen, L.A., Burde, R.M., and Loewy, A.D. (1983). Brainstem connections to the Edinger-Westphal nucleus of the cat: a retrograde tracer study. Brain Res. *261*, 303–306.

Briand, L.A., Gritton, H., Howe, W.M., Young, D.A., and Sarter, M. (2007). Modulators in concert for cognition: modulator interactions in the prefrontal cortex. Prog. Neurobiol. *83*, 69–91.

Chandler, D.J., Gao, W.J., and Waterhouse, B.D. (2014). Heterogeneous organization of the locus coeruleus projections to prefrontal and motor cortices. Proc. Natl. Acad. Sci. USA *111*, 6816–6821.

Chiang, C., and Aston-Jones, G. (1993). Response of locus coeruleus neurons to footshock stimulation is mediated by neurons in the rostral ventral medulla. Neuroscience *53*, 705–715.

de Gee, J.W., Knapen, T., and Donner, T.H. (2014). Decision-related pupil dilation reflects upcoming choice and individual bias. Proc. Natl. Acad. Sci. USA *111*, E618–E625.

Dillier, N., Laszlo, J., Müller, B., Koella, W.P., and Olpe, H.R. (1978). Activation of an inhibitory noradrenergic pathway projecting from the locus coeruleus to the cingulate cortex of the rat. Brain Res. *154*, 61–68.

Donner, T.H., and Siegel, M. (2011). A framework for local cortical oscillation patterns. Trends Cogn. Sci. *15*, 191–199.

Ebitz, R.B., and Platt, M.L. (2015). Neuronal activity in primate dorsal anterior cingulate cortex signals task conflict and predicts adjustments in pupil-linked arousal. Neuron *85*, 628–640.

Edwards, S.B., Ginsburgh, C.L., Henkel, C.K., and Stein, B.E. (1979). Sources of subcortical projections to the superior colliculus in the cat. J. Comp. Neurol. *184*, 309–329.

Einhäuser, W., Stout, J., Koch, C., and Carter, O. (2008). Pupil dilation reflects perceptual selection and predicts subsequent stability in perceptual rivalry. Proc. Natl. Acad. Sci. USA *105*, 1704–1709.

Einhäuser, W., Koch, C., and Carter, O.L. (2010). Pupil dilation betrays the timing of decisions. Front. Hum. Neurosci. *4*, 18.

Eldar, E., Cohen, J.D., and Niv, Y. (2013). The effects of neural gain on attention and learning. Nat. Neurosci. *16*, 1146–1153.

Ennis, M., and Aston-Jones, G. (1988). Activation of locus coeruleus from nucleus paragigantocellularis: a new excitatory amino acid pathway in brain. J. Neurosci. *8*, 3644–3657.

Ennis, M., Aston-Jones, G., and Shiekhattar, R. (1992). Activation of locus coeruleus neurons by nucleus paragigantocellularis or noxious sensory stimulation is mediated by intracoerulear excitatory amino acid neurotransmission. Brain Res. *598*, 185–195.

Foote, S.L., Bloom, F.E., and Aston-Jones, G. (1983). Nucleus locus ceruleus: new evidence of anatomical and physiological specificity. Physiol. Rev. *63*, 844–914.

Gilzenrat, M.S., Nieuwenhuis, S., Jepma, M., and Cohen, J.D. (2010). Pupil diameter tracks changes in control state predicted by the adaptive gain theory of locus coeruleus function. Cogn. Affect. Behav. Neurosci. *10*, 252–269.

Granholm, E., and Steinhauer, S.R. (2004). Pupillometric measures of cognitive and emotional processes. Int. J. Psychophysiol. *52*, 1–6.

Haider, B., and McCormick, D.A. (2009). Rapid neocortical dynamics: cellular and network mechanisms. Neuron *62*, 171–189.

Hajós, M., and Engberg, G. (1990). A role of excitatory amino acids in the activation of locus coeruleus neurons following cutaneous thermal stimuli. Brain Res. *521*, 325–328.

Hayden, B.Y., Heilbronner, S.R., Pearson, J.M., and Platt, M.L. (2011). Surprise signals in anterior cingulate cortex: neuronal encoding of unsigned reward prediction errors driving adjustment in behavior. J. Neurosci. *31*, 4178–4187.

Hayes, T.R., and Petrov, A.A. (2015). Mapping and correcting the influence of gaze position on pupil size measurements. Behav. Res. Methods. Published online May 8, 2015. http://dx.doi.org/10.3758/s13428-015-0588-x.

Heilbronner, S.R., and Haber, S.N. (2014). Frontal cortical and subcortical projections provide a basis for segmenting the cingulum bundle: implications for neuroimaging and psychiatric disorders. J. Neurosci. *34*, 10041–10054.

Hormigo, S., Horta Júnior, Jde.A., Gómez-Nieto, R., and López, D.E. (2012). The selective neurotoxin DSP-4 impairs the noradrenergic projections from the locus coeruleus to the inferior colliculus in rats. Front. Neural Circuits *6*, 41.

Hou, R.H., Freeman, C., Langley, R.W., Szabadi, E., and Bradshaw, C.M. (2005). Does modafinil activate the locus coeruleus in man? Comparison of modafinil and clonidine on arousal and autonomic functions in human volunteers. Psychopharmacology (Berl.) *181*, 537–549.

Hunter, J.D., Milton, J.G., Lüdtke, H., Wilhelm, B., and Wilhelm, H. (2000). Spontaneous fluctuations in pupil size are not triggered by lens accommodation. Vision Res. *40*, 567–573.

Jepma, M., and Nieuwenhuis, S. (2011). Pupil diameter predicts changes in the exploration-exploitation trade-off: evidence for the adaptive gain theory. J. Cogn. Neurosci. *23*, 1587–1596.

Kahneman, D., and Beatty, J. (1966). Pupil diameter and load on memory. Science *154*, 1583–1585.

Kalwani, R.M., Bloy, L., Elliott, M.A., and Gold, J.I. (2009). A method for localizing microelectrode trajectories in the macaque brain using MRI. J. Neurosci. Methods *176*, 104–111.

Kalwani, R.M., Joshi, S., and Gold, J.I. (2014). Phasic activation of individual neurons in the locus ceruleus/subceruleus complex of monkeys reflects rewarded decisions to go but not stop. J. Neurosci. *34*, 13656–13669.

Klepper, A., and Herbert, H. (1991). Distribution and origin of noradrenergic and serotonergic fibers in the cochlear nucleus and inferior colliculus of the rat. Brain Res. *557*, 190–201.

Kopell, N., Ermentrout, G.B., Whittington, M.A., and Traub, R.D. (2000). Gamma rhythms and beta rhythms have different synchronization properties. Proc. Natl. Acad. Sci. USA *97*, 1867–1872.

Krekelberg, B. (2011). Microsaccades. Curr. Biol. *21*, R416.

Krugman, H.E. (1964). Some applications of pupil measurement. J. Mark. Res. *1*, 15–19.

Lavín, C., San Martín, R., and Rosales Jubal, E. (2014). Pupil dilation signals uncertainty and surprise in a learning gambling task. Front. Behav. Neurosci. *7*, 218.

Lee, S.H., and Dan, Y. (2012). Neuromodulation of brain states. Neuron *76*, 209–222.

Lee, C.R., and Tepper, J.M. (2009). Basal ganglia control of substantia nigra dopaminergic neurons. J. Neural Transm. Suppl. *73*, 71–90.

Levitt, P., and Moore, R.Y. (1978). Noradrenaline neuron innervation of the neocortex in the rat. Brain Res. *139*, 219–231.

Loewenfeld, I.E. (1999). The Pupil: Anatomy, Physiology, and Clinical Applications (Butterworth and Heinemann).

Loewenfeld, I.E., and Newsome, D.A. (1971). Iris mechanics. I. Influence of pupil size on dynamics of pupillary movements. Am. J. Ophthalmol. *71*, 347–362.

Martinez-Conde, S., Otero-Millan, J., and Macknik, S.L. (2013). The impact of microsaccades on vision: towards a unified theory of saccadic function. Nat. Rev. Neurosci. *14*, 83–96.

McGinley, M.J., David, S.V., and McCormick, D.A. (2015). Cortical membrane potential signature of optimal states for sensory signal detection. Neuron *87*, 179–192.

Morad, Y., Lemberg, H., Yofe, N., and Dagan, Y. (2000). Pupillography as an objective indicator of fatigue. Curr. Eye Res. *21*, 535–542.

Murphy, P.R., Robertson, I.H., Balsters, J.H., and O'Connell, R.G. (2011). Pupillometry and P3 index the locus coeruleus-noradrenergic arousal function in humans. Psychophysiology *48*, 1532–1543.

Murphy, P.R., O'Connell, R.G., O'Sullivan, M., Robertson, I.H., and Balsters, J.H. (2014). Pupil diameter covaries with BOLD activity in human locus coeruleus. Hum. Brain Mapp. *35*, 4140–4154.

Mysore, S.P., and Knudsen, E.I. (2013). A shared inhibitory circuit for both exogenous and endogenous control of stimulus selection. Nat. Neurosci. *16*, 473–478.

Nassar, M.R., Rumsey, K.M., Wilson, R.C., Parikh, K., Heasly, B., and Gold, J.I. (2012). Rational regulation of learning dynamics by pupil-linked arousal systems. Nat. Neurosci. *15*, 1040–1046.

Nieuwenhuis, S., De Geus, E.J., and Aston-Jones, G. (2011). The anatomical and functional relationship between the P3 and autonomic components of the orienting response. Psychophysiology *48*, 162–175.

Paukert, M., Agarwal, A., Cha, J., Doze, V.A., Kang, J.U., and Bergles, D.E. (2014). Norepinephrine controls astroglial responsiveness to local circuit activity. Neuron *82*, 1263–1270.

Paxinos, G., Huang, X.-F., Petrides, M., and Toga, A. (2008). The Rhesus Monkey Brain in Stereotaxic Coordinates, Second Edition (Academic Press).

Phillips, M.A., Szabadi, E., and Bradshaw, C.M. (2000). Comparison of the effects of clonidine and yohimbine on pupillary diameter at different illumination levels. Br. J. Clin. Pharmacol. *50*, 65–68.

Polack, P.O., Friedman, J., and Golshani, P. (2013). Cellular mechanisms of brain state-dependent gain modulation in visual cortex. Nat. Neurosci. *16*, 1331–1339.

Porrino, L.J., and Goldman-Rakic, P.S. (1982). Brainstem innervation of prefrontal and anterior cingulate cortex in the rhesus monkey revealed by retrograde transport of HRP. J. Comp. Neurol. *205*, 63–76.

Preuschoff, K., 't Hart, B.M., and Einhäuser, W. (2011). Pupil dilation signals surprise: evidence for noradrenaline's role in decision making. Front. Neurosci. *5*, 115.

Reimer, J., Froudarakis, E., Cadwell, C.R., Yatsenko, D., Denfield, G.H., and Tolias, A.S. (2014). Pupil fluctuations track fast switching of cortical states during quiet wakefulness. Neuron *84*, 355–362.

Richer, F., and Beatty, J. (1987). Contrasting effects of response uncertainty on the task-evoked pupillary response and reaction time. Psychophysiology *24*, 258–262.

Robinson, D.A. (1972). Eye movements evoked by collicular stimulation in the alert monkey. Vision Res. *12*, 1795–1808.

Salinas, E., and Sejnowski, T.J. (2001). Gain modulation in the central nervous system: where behavior, neurophysiology, and computation meet. Neuroscientist *7*, 430–440.

Sara, S.J., and Bouret, S. (2012). Orienting and reorienting: the locus coeruleus mediates cognition through arousal. Neuron *76*, 130–141.

Schmidt, H.S., and Fortin, L.D. (1982). Electronic pupillography in disorders of arousal. In Sleeping and Waking Disorders: Indication and Technique, L.D. Fortin, H.S. Schmidt, and C. Guilleminault, eds. (Addison-Wesley), pp. 127–143.

Schwarz, L.A., Miyamichi, K., Gao, X.J., Beier, K.T., Weissbourd, B., DeLoach, K.E., Ren, J., Ibanes, S., Malenka, R.C., Kremer, E.J., and Luo, L. (2015). Viral-genetic tracing of the input-output organization of a central noradrenaline circuit. Nature *524*, 88–92.

Segal, M., and Bloom, F.E. (1976). The action of norepinephrine in the rat hippocampus. III. Hippocampal cellular responses to locus coeruleus stimulation in the awake rat. Brain Res. *107*, 499–511.

Servan-Schreiber, D., Printz, H., and Cohen, J.D. (1990). A network model of catecholamine effects: gain, signal-to-noise ratio, and behavior. Science *249*, 892–895.

Shadlen, M.N., Britten, K.H., Newsome, W.T., and Movshon, J.A. (1996). A computational analysis of the relationship between neuronal and behavioral responses to visual motion. J. Neurosci. *16*, 1486–1510.

Sharma, Y., Xu, T., Graf, W.M., Fobbs, A., Sherwood, C.C., Hof, P.R., Allman, J.M., and Manaye, K.F. (2010). Comparative anatomy of the locus coeruleus in humans and nonhuman primates. J. Comp. Neurol. *518*, 963–971.

Sparks, D.L., and Nelson, J.S. (1987). Sensory and motor maps in the mammalian superior colliculus. Trends Neurosci. *10*, 312–317.

Stanten, S.F., and Stark, L. (1966). A statistical analysis of pupil noise. IEEE Trans. Biomed. Eng. *13*, 140–152.

Stark, L.R., and Atchison, D.A. (1997). Pupil size, mean accommodation response and the fluctuations of accommodation. Ophthalmic Physiol. Opt. *17*, 316–323.

Takeuchi, T., Puntous, T., Tuladhar, A., Yoshimoto, S., and Shirama, A. (2011). Estimation of mental effort in learning visual search by measuring pupil response. PLoS ONE *6*, e21973.

Van Bockstaele, E.J., Colago, E.E., and Aicher, S. (1998). Light and electron microscopic evidence for topographic and monosynaptic projections from neurons in the ventral medulla to noradrenergic dendrites in the rat locus coeruleus. Brain Res. *784*, 123–138.

Varazzani, C., San-Galli, A., Gilardeau, S., and Bouret, S. (2015). Noradrenaline and dopamine neurons in the reward/effort trade-off: a direct electrophysiological comparison in behaving monkeys. J. Neurosci. *35*, 7866–7877.

Vinck, M., Batista-Brito, R., Knoblich, U., and Cardin, J.A. (2015). Arousal and locomotion make distinct contributions to cortical activity patterns and visual encoding. Neuron *86*, 740–754.

Vogt, B.A., Hof, P.R., Friedman, D.P., Sikes, R.W., and Vogt, L.J. (2008). Norepinephrinergic afferents and cytology of the macaque monkey midline, mediodorsal, and intralaminar thalamic nuclei. Brain Struct. Funct. *212*, 465–479.

von Stein, A., and Sarnthein, J. (2000). Different frequencies for different scales of cortical integration: from local gamma to long range alpha/theta synchronization. Int. J. Psychophysiol. *38*, 301–313.

Wang, C.A., and Munoz, D.P. (2015). A circuit for pupil orienting responses: implications for cognitive modulation of pupil size. Curr. Opin. Neurobiol. *33*, 134–140.

Wang, Y., Luksch, H., Brecha, N.C., and Karten, H.J. (2006). Columnar projections from the cholinergic nucleus isthmi to the optic tectum in chicks (Gallus gallus): a possible substrate for synchronizing tectal channels. J. Comp. Neurol. *494*, 7–35.

Wang, C.A., Boehnke, S.E., White, B.J., and Munoz, D.P. (2012). Microstimulation of the monkey superior colliculus induces pupil dilation without evoking saccades. J. Neurosci. *32*, 3629–3636.

Wang, C.A., Boehnke, S.E., Itti, L., and Munoz, D.P. (2014). Transient pupil response is modulated by contrast-based saliency. J. Neurosci. *34*, 408–417.

Warga, M., Lüdtke, H., Wilhelm, H., and Wilhelm, B. (2009). How do spontaneous pupillary oscillations in light relate to light intensity? Vision Res. *49*, 295–300.

Waterhouse, B.D., Moises, H.C., and Woodward, D.J. (1980). Noradrenergic modulation of somatosensory cortical neuronal responses to iontophoretically applied putative neurotransmitters. Exp. Neurol. *69*, 30–49.

Yu, A.J., and Dayan, P. (2005). Uncertainty, neuromodulation, and attention. Neuron *46*, 681–692.